Author Manuscript

Author Manuscript

Author Manuscript

Author Manuscript

HHS Public Access

Author manuscript

Nat Commun. Author manuscript; available in PMC 2015 March 18.

Published in final edited form as:

Nat Commun. ; 5: 4896. doi:10.1038/ncomms5896.

Structural analyses of Ca^{2+}/CaM interaction with Na_V channel C-termini reveal mechanisms of calcium-dependent regulation

Chaojian Wang[1,2,*], **Ben C. Chung**[1,3,*], **Haidun Yan**[1,2], **Hong-Gang Wang**[1,2], **Seok-Yong Lee**[1,3], and **Geoffrey S. Pitt**[1,2,4]

[1]Ion Channel Research Unit, Duke University Medical Center, 2 Genome Ct, Durham, North Carolina, 27710, USA

[2]Division of Cardiology, Department of Medicine, Duke University Medical Center, 2 Genome Ct, Durham, North Carolina, 27710, USA

[3]Department of Biochemistry, Duke University Medical Center, 2 Genome Ct, Durham, North Carolina, 27710, USA

[4]Department of Pharmacology, Duke University Medical Center, 2 Genome Ct, Durham, North Carolina, 27710, USA

Abstract

Ca^{2+} regulates voltage-gated Na^+ (Na_V) channels and perturbed Ca^{2+} regulation of Na_V function is associated with epilepsy syndromes, autism, and cardiac arrhythmias. Understanding the disease mechanisms, however, has been hindered by a lack of structural information and competing models for how Ca^{2+} affects Na_V channel function. Here, we report the crystal structures of two ternary complexes of a human Na_V cytosolic C-terminal domain (CTD), a fibroblast growth factor homologous factor, and Ca^{2+}/calmodulin (Ca^{2+}/CaM). These structures rule out direct binding of Ca^{2+} to the Na_V CTD, and uncover new contacts between CaM and the Na_V CTD. Probing these new contacts with biochemical and functional experiments allows us to propose a mechanism by which Ca^{2+} could regulate Na_V channels. Further, our model provides hints towards understanding the molecular basis of the neurologic disorders and cardiac arrhythmias caused by Na_V channel mutations.

Users may view, print, copy, and download text and data-mine the content in such documents, for the purposes of academic research, subject always to the full Conditions of use:http://www.nature.com/authors/editorial_policies/license.html#terms

Correspondence and requests for materials should be addressed to: G.S. Pitt, geoffrey.pitt@duke.edu, tel: 919-668-7641, fax: 919-613-5145, S.-Y. Lee, sylee@biochem.duke.edu, tel: 919-684-1005, fax: 919-613-5145.

*These authors contributed equally to this work.

Author contributions: S-YL and GSP designed the study. CW, BCC, HY, and H-GG performed experiments. All authors analyzed data. S-YL and GSP wrote the manuscript.

Accession Numbers: Atomic coordinates and structure factors for the reported crystal structures have been deposited in the Protein Data Bank under accession codes 4JPZ and 4JQ0, for the $Na_V1.2/Ca^{2+}$ and $Na_V1.5/Ca^{2+}$ structures, respectively.

Competing financial interest: The authors declare no competing financial interests.

Author Manuscript Author Manuscript Author Manuscript Author Manuscript

Introduction

Na_V channels underlie the rapid upstroke of action potentials. Mammalian Na_V channels are pseudotetramers with 6-transmembrane segment repeats joined by intracellular linkers and flanked by intracellular N- and C-termini. The four repeats, which each contain a voltage sensor, assemble to form a central pore. Although recent crystal structures of the tetrameric bacterial Na_V channel from *Arcobacter butzleri* (NavAb) provided detail about the pore and voltage sensors [1, 2], NavAb tetramers lack the intracellular linkers and termini of mammalian Na_V channels. Those components are of particular interest because they confer isoform-specific regulatory effects, serve as sites of interaction for critical modulatory proteins, and are loci for many disease-causing mutations.

The C-terminal domain (CTD) is of particular interest because it exerts powerful effects upon channel inactivation [3] and is the interaction site for several auxiliary proteins that modulate channel function, such as calmodulin (CaM) and fibroblast growth factor homologous factors (FHFs), both of which regulate excitability through their CTD interactions [4, 5]. Moreover, many disease-causing mutations localize to Na_V CTDs or their associated proteins. Key examples include mutations in *SCN1A* and *SCN2A* (which encode the neuronal channels $Na_V1.1$ and $Na_V1.2$, respectively) that lead to various epilepsy syndromes, ataxia, and autism [6, 7, 8] or in the CTD of $Na_V1.5$, the cardiac Na_V channel encoded by *SCN5A*, which is a hotspot for mutations causing arrhythmias, cardiomyopathy, and sudden infant death syndrome [9, 10, 11, 12, 13, 14]. Likewise, mutations in FHFs or CaM have been associated with neurodegenerative disorders, cognitive deficits, and arrhythmias [14, 15, 16]. Structural information about Na_V CTDs, however, has been limited. How the associated regulatory proteins influence channel function and how mutations in the CTDs or associated auxiliary proteins perturb channel function and at the molecular level are not well understood.

Among the proteins associated with Na_V CTDs CaM is of particular interest because it acts as a sensor for Ca^{2+}, which serves as a critical signal of electrical activity, providing powerful feedback regulation upon Na_V channel function [17]. Still, how Ca^{2+} and CaM affect Na_V channels have been controversial since sequence analysis of Na_V channels first revealed the presence of potential CaM-binding sites, including an “IQ” motif [5] and a potential Ca^{2+} binding site within the CTD [18]. Obtaining an understanding for CaM regulation of Na_V channels has been further complicated by apparent isoform-specific regulation. For example, CaM affects inactivation properties of the neuronal $Na_V1.6$ but not the skeletal muscle $Na_V1.4$ [19]. For the cardiac $Na_V1.5$, CaM affects several different properties, including channel inactivation and persistent current [20, 21]. Nevertheless, the identification of disease-causing mutations within or near the Na_V IQ motifs of several Na_V isoforms [6, 20, 22, 23, 24] highlights important roles for CaM. The potential significance of CaM-binding to Na_V channels has been further spotlighted by recent exome sequencing studies in which searches for repeated rare variants or *de novo* mutations associated with autism identified *SCN1A* and *SCN2A* among the small list of loci [25, 26, 27]; several of these cataloged Na_V mutations cluster in and around the IQ motif.

Author Manuscript Author Manuscript Author Manuscript Author Manuscript

A major barrier to understanding how Ca^{2+} and CaM act on Na_V channels has been that structural information is limited to Ca^{2+}-free CaM (apoCaM) interacting with the CTD. While such studies defined an interaction between the decalcified C-lobe of CaM and the IQ motif [28, 29, 30], those structures were unable to reveal how Ca^{2+} affects Na_V function and did not provide insight into mechanisms for IQ motif disease mutations, including a familial autism mutation in the neuronal $Na_V1.2$ channel [7] and a cardiac arrhythmia mutation in the cardiac $Na_V1.5$ [20] that fall outside of the apoCaM contact sites.

Here, we present crystal structures of $Na_V1.2$ and $Na_V1.5$ CTDs bound to Ca^{2+}–CaM. Comparison with our previous structure obtained with apoCaM reveals novel and unexpected Ca^{2+}–CaM contacts and stark differences in the overall conformation of the ternary complex, including a Ca^{2+}-dependent interaction between the CaM N-lobe and an extended helix that contains the IQ motif. Together, these findings provide a basis for understanding the effects of specific disease-causing mutations within Na_V CTD domains.

Results

Ternary complex structures of a Na_V CTD, FHF, and Ca^{2+}/CaM

To define how Ca^{2+} regulates Na_V channels, we solved crystal structures of complexes containing a Na_V CTD, Ca^{2+}–CaM, and a FHF. FHFs are constitutive Na_V subunits in brain [4, 31] and heart [32] and their inclusion allows us to compare Ca^{2+}/CaM structures with our previous complex containing apoCaM [30]. We tested several different combinations of FHFs and Na_V CTDs with Ca^{2+}/CaM and eventually succeeded in crystallizing two ternary complexes: a 6xHis-tagged human $Na_V1.5$ CTD (amino acids 1773-1940), human FGF12B, and CaM; and a 6xHis-tagged human $Na_V1.2$ CTD (amino acids 1777-1937), human FGF13U, and CaM. The sequences of the Na_V CTDs are highly conserved among the subtypes (76% identities between $Na_V1.5$ and $Na_V1.2$, and 91% of the amino acids are conserved; Fig. 1a) and the solution structures of the proximal $Na_V1.2$ CTD and $Na_V1.5$ CTD are nearly identical [33, 34]. Likewise, FGF12B and FGF13U are highly conserved (69% identities), and their crystal structures in the absence of any binding partners are similar [35]. Thus, we anticipated significant similarities between the $Na_V1.2$- and $Na_V1.5$-containing complexes.

Both complexes were expressed in *E. coli* and purified in the presence of 2 mM Ca^{2+} by Co^{2+} affinity chromatography followed by size exclusion chromatography. The two ternary complexes (combined M_w ~60 kDa) were stable and each eluted in a single peak on a size exclusion column (Supplementary Fig. 1). Their individual profiles were highly similar to each other and to what we observed for the ternary complex containing the $Na_V1.5$ CTD, FGF13U, and CaM purified in EGTA, for which we had demonstrated a stoichiometry of 1:1:1 [30].

The complex containing $Na_V1.2$ CTD, FGF13U, and CaM (hereafter referred to as $Na_V1.2/Ca^{2+}$) was crystallized in the C2 space group with two copies of the ternary complex in each asymmetric unit. The crystals were grown in the presence of 2 mM Ca^{2+} and diffracted to 3.02 Å Bragg spacings. The experimental phases were derived by single anomalous dispersion from selenomethionine-substituted crystals and improved by two-fold

Author Manuscript Author Manuscript Author Manuscript Author Manuscript

non-crystallographic averaging, which yielded a good-quality electron density map (Supplementary Fig. 2a). The final model contains the $Na_V1.2$ amino acids 1788-1929, FGF13U amino acids 11-158, and the CaM amino acids 7-149. The model was refined to R_{work}/R_{free} of 21.5/24.6 % (Table 1). The ternary complex containing $Na_V1.5$ CTD, FGF12B, and CaM (hereafter referred to as $Na_V1.5/Ca^{2+}$) was crystallized in the $P3_121$ space group with one copy of the ternary complex in each asymmetric unit. The crystals were grown in the presence of 2 mM Ca^{2+} and diffracted anisotropically to 3.8/5.4/6.0 Å Bragg spacings. Molecular replacement was performed to obtain the phases (see Methods for the details). The final model contains the $Na_V1.5$ amino acids 1786-1927; FGF12B amino acids 12-152; and the CaM amino acid 7-148. Despite the resolution limit, the model refined to good statistics (R_{work}/R_{free} of 26.2/31.8 %) and good geometry (Table 1 and Methods for the refinement). 2Fo-Fc OMIT map shows a good-quality electron density, supporting the accuracy of the model given the resolution (Supplementary Fig. 2B). There is no significant difference in the refinement statistics when the data was truncated to 6.0 Å (Table 1).

Figure 1B-C show the overall architecture of the $Na_V1.2/Ca^{2+}$ and $Na_V1.5/Ca^{2+}$ ternary complexes, respectively. In both complexes, the Na_V CTD is comprised of one globular domain that contains an EF-hand fold followed by an extended helix that contains the IQ motif. We refer to this helix as the IQ domain. The FHF binds to the CTD globular domain and CaM binds to the IQ domain. When the $Na_V1.5/Ca^{2+}$ and the $Na_V1.2/Ca^{2+}$ structures were superimposed with respect to their IQ domain, structural conservation was observed within the region containing the IQ domain and CaM (r.m.s.d. of 1.7 Å) (Fig. 1D).

When the two structures (stripped of their respective CaM molecules) are superimposed relative to their respective CTD's globular domains together with FHFs, both Na_V CTD globular domains and FHFs are very similar with the r.m.s.d of 0.89 Å, with their IQ domains out of register (Fig. 1E) due to different angles between their CTD's globular domain (along with FHFs) and their IQ domain. The different angle may reflect an isoform-specific structural difference or inherent flexibility between the two domains of Na_V CTD.

To focus on the Ca^{2+} dependent conformational changes, we also superimposed our previously solved structure of a ternary complex of $Na_V1.5$ CTD, FGF13, and CaM crystalized in the absence of Ca^{2+} [30], hereafter referred to as $Na_V1.5/\text{-}Ca^{2+}$. With the CaM molecules stripped for clarity, Fig. 1E shows that the difference in angle between the respective Na_V CTD globular domains and the IQ domains is even more pronounced between $Na_V1.5/Ca^{2+}$ and $Na_V1.5/\text{-}Ca^{2+}$ than between $Na_V1.2/Ca^{2+}$ and $Na_V1.5/Ca^{2+}$ (Fig. 1E). Although it is possible that these rigid-body motions between the CTD globular domains and their respective IQ domains are associated with Ca^{2+} binding, these motions can also be due to inherent flexibility between these two domains. Because the $Na_V1.2/Ca^{2+}$ structure provides higher resolution than the $Na_V1.5/Ca^{2+}$ structure and the differences are otherwise minimal, subsequent analyses focus only on the $Na_V1.2/Ca^{2+}$ structure.

A Ca^{2+}-dependent CaM N-lobe interaction with the IQ domain

The most significant effects of Ca^{2+} are the changes in the interactions between CaM and the respective IQ domains as shown in Figure 2A, B, in which the $Na_V1.2/Ca^{2+}$ and

Author Manuscript Author Manuscript Author Manuscript Author Manuscript

$Na_V1.5$/-Ca^{2+} structures are aligned by their IQ domains. The CaM in the $Na_V1.5$/-Ca^{2+} structure adopts an extended conformation with the α-helical interlobular linker between the CaM/N- and C-lobes holding the N-lobe away from the C-lobe that binds to the proximal portion (IQ motif) of the IQ domain. NMR structures of Ca^{2+}-free CaM and an isolated IQ domain peptide from either $Na_V1.2$ or $Na_V1.5$ also showed an interaction between the CaM C-lobe and the IQ motif, but not the CaM N/lobe and the IQ domain [28, 29]. In our new $Na_V1.2$/Ca^{2+} structure, in contrast, the α-helical interlobular linker is unwound, thereby allowing the Ca^{2+}-bound CaM N-lobe to envelope the distal portion of the IQ domain and provide additional contacts between the linker and the IQ domain and between the CaM N-lobe and the IQ domain that are not present in the absence of Ca^{2+}. These new contacts include residues mutated in channelopathies, as discussed below.

Superposition of $Na_V1.5$/-Ca^{2+} and $Na_V1.2$/Ca^{2+} structures shows that there are only minor conformational changes with respect to CaM C-lobe. In both structures, the CaM C-lobe adopts the “semi-open” conformation (Fig. 2C) that was first described for apoCaM bound to an IQ motif from an unconventional myosin [36]. Significant conformational changes, however, occurred within the N-lobe of CaM, which assumes a “closed” conformation in the $Na_V1.2$/Ca^{2+} structure (Fig. 2C and 2D), similar to the conformation observed for the N-lobe of Ca^{2+}/CaM bound to its target peptide in CaMKII [37]. For comparison, in the $Na_V1.5$/-Ca^{2+} structure the unbound CaM N-lobe displays the “semi-open” conformation [30]. Additionally, the arrangement of CaM lobes with respect to the IQ domain is novel to the best of our knowledge (see Discussion for the further details).

These conformation differences of the individual CaM lobes in the $Na_V1.2$/Ca^{2+} structure suggested that the C-lobe was unlikely to be fully occupied while the N-lobe is saturated with Ca^{2+}. To test this hypothesis we collected data for the $Na_V1.2$/Ca^{2+} crystals at a long wavelength (1.55 Å), for which the anomalous scattering power of Ca^{2+} (f″ ∼1.2 e) is higher than that of sulfur (∼0.6 e) while that of Mg^{2+} is nearly silent (∼0.1 e). Although we observed strong anomalous difference Fourier peaks in the Ca^{2+}-binding loops of the CaM N-lobes, only weak peaks were observed in the Ca^{2+}-binding loops of the CaM C-lobe (Supplementary Fig. 3), suggesting that the affinity for Ca^{2+} in the CaM C-lobe of $Na_V1.2$/Ca^{2+} is low (compared to the CaM N-lobe) and that the CaM C-lobe is only partially occupied with Ca^{2+}, consistent with the semi-open conformation of the CaM C-lobe.

This newly discovered interaction between the CaM N-lobe and the distal C-terminal portion of the IQ domain is driven mainly through van der Waals forces (Fig. 2E), burying $Na_V1.2$ hydrophobic side chains (Leu1920, Leu1921, Val1925, and Val1928) and has functional and disease-related implications. First, this additional interaction between the distal IQ domain and the CaM N-lobe offers an explanation for a previous report that an Ala1924Thr mutation in the cardiac $Na_V1.5$ channel (equivalent to Val1928 in $Na_V1.2$) causes the life-threatening arrhythmia Brugada Syndrome and eliminates the Ca^{2+}/CaM-dependent slow inactivation observed for the wild-type $Na_V1.5$ channel [20]. We hypothesized that the Ala1924Thr mutation in the $Na_V1.5$ CTD affected the affinity for Ca^{2+}/CaM, and tested the hypothesis by isothermal calorimetry (ITC). Indeed, in the presence of saturating 5 mM Ca^{2+}, the mutation reduced the affinity for Ca^{2+}/CaM by ∼ 3-fold compared to the

Author Manuscript Author Manuscript Author Manuscript Author Manuscript

wild-type $Na_V1.5$ CTD (Supplementary Fig. 4A and Table 2). In contrast, the affinity of the mutant $Na_V1.5$ CTD for CaM in the absence of Ca^{2+} was mildly increased (Table 2). Second, we found that the CaM N-lobe interaction with the distal IQ domain provides a significant boost to the affinity of Ca^{2+}/CaM for the Na_V CTD. A previous report using ITC [38] had found the affinity of Ca^{2+}/CaM for a $Na_V1.5$ peptide containing the IQ motif to be ~ 2.1 μM. Those thermodynamic parameters, however, were obtained in experiments employing an IQ domain in which the newly discovered CaM N-lobe contact site is truncated. We therefore performed ITC with a longer $Na_V1.5$ CTD (through amino acid 1940), and observed a significantly higher affinity for both Ca^{2+}/CaM and apoCaM (~100 nM, as shown in Supplementary Fig. 4A-B and Table 2). To assure that the lower K_d values we obtained were indeed due to the longer CTD and not to technical differences, we measured the affinity of CaM for the $Na_V1.5$ CTD truncated at amino acid 1924, for which we obtained a value of 2.0 ± 0.4 μM in 5 mM Ca^{2+} (Table 2 and Supplementary Fig. 4B). This result is in excellent agreement with the value previously obtained [38], thereby allowing us to benchmark our thermodynamic data against that report. Thus, the ~ 20-fold higher affinity for CaM obtained with the longer CTD highlights critical contributions of the more distal IQ domain residues. Comparison of the N values of interactions for Ca^{2+}/CaM with the two CTDs by ITC (Table 2) further demonstrates the importance of the more distal residues in the IQ domain. For the shorter CTD, the N value of the Ca^{2+}/CaM-CTD interaction is close to ~0.5 (0.38 in our measurement; and 0.56 previously reported [38]), suggesting that one Ca^{2+}/CaM can bind two CTDs. The N value we obtained for the longer CTD was doubled (0.84), suggesting that one Ca^{2+}/CaM binds one CTD, and fits well with our crystallographic observation that both N- and C-lobes simultaneously bind to different sites within the IQ domain of Na_V CTD. Consistent with our observation, N value of the interaction between Ca^{2+}/CaM and Ala1924Thr of the longer CTD is reduced to half of the wild type (0.42) (Table 2). Thus, these data underlined the importance of the interaction between CaM and the more distal region of the IQ domain and supported a model in which there are simultaneous interactions of the two CaM lobes (at different sites on the IQ domain).

Ca^{2+}-dependent changes and disease mechanisms

While the new CaM N-lobe contact with the $Na_V1.2$ CTD is the most obvious Ca^{2+}-dependent structural change, we also identified additional new Ca^{2+}/CaM contact sites within the $Na_V1.2$ IQ domain, which may provide insight for several other Na_V channelopathies. For example, Arg1918 (Fig. 3A, B), which contacts Asp79 and Ser82 in the CaM interlobular linker in the Ca^{2+}-loaded complex (but not in the apoCaM structure), was reported in a patient with febrile seizures and childhood absence epilepsy [23], and mutation of the equivalent Arg1928 in the homologous $Na_V1.1$ was found in a patient with severe myoclonic epilepsy of infancy [24].

Also of particular interest was a familial autism mutation Arg1902Cys in $Na_V1.2$ [7], particularly since recent analyses of rare *de novo* mutations in subjects with autism have identified *SCN2A* as one of a handful of high-confidence autism spectrum disorder genes [25, 39]. Arg1902 sits at the hinge between the CTD globular domain and the IQ domain helix (Fig. 3C). We had previously found that the Arg1902Cys mutation conferred a Ca^{2+}/

Author Manuscript Author Manuscript Author Manuscript Author Manuscript

CaM-dependent conformational change indicated by a significant Ca^{2+}-dependent shift in migration on a size exclusion column of a $Na_V1.2$ CTD/CaM binary complex that was not observed with the wild type complex [21]. Although Arg1902 (or the Arg1898 equivalent in $Na_V1.5$) does not make any direct contacts with CaM either in the presence or absence of Ca^{2+}, it interacts with the side chain of Glu1905 (Glu1901 in $Na_V1.5$) one turn below along the IQ domain helix and also forms cation-π interaction with the side chain of Tyr98 in FGF13 in the $Na_V1.5$/-Ca^{2+} structure. Tyr98 in FGF13 and Glu1905 in $Na_V1.2$ (Glu1901 in $Na_V1.5$) also interact with Lys95 within the third CaM EF-hand in the CaM C-lobe. Interestingly, Glu1905 in $Na_V1.2$, Tyr98 in FGF13, and Lys95 in CaM are the only residues within the ternary complex that make interactions with each of the other partners. Thus, we suspected that the relayed interactions from Lys95 (CaM) through Glu1905 (Nav IQ domain) to Arg1902 (Nav globular domain), stabilized by the cation-π interaction with Tyr98 in FGF13, suppress the Ca^{2+} dependence of $Na_V1.2$ channels and that disruption of these interactions would affect Ca^{2+}-dependent regulation of $Na_V1.2$ channels (Fig. 3C). We tested this hypothesis in two ways.

First, we expressed either wild type or Arg1902Cys mutant $Na_V1.2$ along with FGF14, the best characterized neuronal FHF [4, 31, 40] in HEK293 cells, in which endogenous CaM is abundant, and recorded Na^+ currents in the presence of saturating internal Ca^{2+} or nominally zero internal Ca^{2+} (Supplementary Fig. 5) For wild type NaV1.2, inclusion of 10 μM Ca^{2+} in the patch pipette did not affect peak current density, the V1/2 of activation, or the V1/2 of steady-state inactivation. In contrast, for the Arg1902Cys mutant the addition of Ca^{2+} induced a large ∼-10 mV shift in the V1/2 of steady-state activation and inactivation (Fig. 3D, Supplementary Fig. 6A, and Supplementary Table 1). To test further our hypothesis that disruption of the Na_V CTD to CaM relay affected Ca^{2+}-dependent regulation of $Na_V1.2$, we ablated the key intermediary by mutating $Na_V1.2$ Glu1905 to Gln. Recordings from the Glu1905Gln mutant channels phenocopied those from the Arg1902Cys mutant channels (Supplementary Fig. 6A and Supplementary Table 1). Second, to test the proposed role of Arg1902 in the relayed interactions in $Na_V1.2$ CTD/apoCaM, we measured the affinity of apoCaM for the wild type and Arg1902Cys mutant $Na_V1.2$ CTDs by ITC. Consistent with our hypothesis, the Arg1902Cys mutation reduced affinity of apoCaM for the $Na_V1.2$ CTD significantly (Table 3 and Supplementary Fig. 4C). We did not observe a difference in affinity for Ca^{2+}/CaM between the wild type and the Arg1902Cys mutant CTD (Table 3 and Supplementary Fig. 4D). Because our ITC measurement in the presence of Ca^{2+} could be complicated by an additional binding process due to Ca^{2+}-loading of the CaM C-lobe, which is essentially unoccupied in the $Na_V1.2$/+Ca^{2+} structure (Supplementary Fig. 3), we therefore prepared CaM in which the third and fourth EF hands were mutated to ablate Ca^{2+} binding to the CaM C-lobe [41] and repeated the ITC measurements with this crippled CaM_{34} mutant. The ITC experiment with the CaM_{34} mutant showed a reduced affinity for the Arg1902Cys mutant compared to the wild CTD in the presence of Ca^{2+} (Table 3 and Supplementary Fig. 4E). Thus these data are consistent with the previously observed shift in mobility on gel filtration of the Arg1902Cys/CaM binary complex [21] and suggest that by disrupting the relayed interactions to CaM the familial autism $Na_V1.2$ Arg1902Cys mutation revealed Ca^{2+}-dependent effects upon channel function that were suppressed in the wild type channel.

Author Manuscript Author Manuscript Author Manuscript Author Manuscript

We next investigated whether the Ca^{2+}-dependent interaction of the CaM N lobe was required for the Ca^{2+}-dependent regulation of $Na_V1.2$ exposed by the Arg1902Cys mutation. We mutated Val1925, one of the $Na_V1.2$ hydrophobic side chains buried by the calcified CaM N lobe (see Fig. 2E), to Lys and examined how this mutant affected the Ca^{2+}-dependent shift in activation and steady-state inactivation in the context of the Arg1902Cys mutant. With this additional Val1925Lys mutation, The Arg1902Cys mutant no longer displayed any Ca^{2+}-dependent effects on either activation or steady-state inactivation (Supplementary Fig. 6B and Supplementary Table 1), thereby implicating a requirement for the interaction between the calcified CaM N lobe and $Na_V1.2$. When analyzed independently, Val1925Lys did not expose any Ca^{2+}-dependent regulation (Supplementary Fig. 6B and Supplementary Table 1).

Ca^{2+} binding is restricted to calmodulin

Our analyses suggested that Ca^{2+}-dependent regulation of Na_V channel function derives from Ca^{2+}-dependent changes in the interaction between CaM and the Na_V CTD, yet it has previously been suggested that Ca^{2+} also affects Na_V channels by binding directly to an EF-hand motif within the Na_V CTD influences Na_V channel function [18, 34, 42]. To query whether Ca^{2+} can bind directly to the Na_V CTD EF-hand motif, we used our anomalous scattering studies. Even though we detected anomalous difference signals from many sulfur atoms (in methionines) whose signal is ~2-fold weaker than that for Ca^{2+}, we did not detect anomalous difference signal for Ca^{2+} within the proposed Ca^{2+}-binding loops (Fig. 4A) and we observed a strong signal for Ca^{2+} bound to the CaM N-lobe (Supplementary Fig. 3). Comparing the acidic and polar residues proposed to coordinate Ca^{2+} in the putative Na_V CTD EF-hand [18] with those in the Ca^{2+}-binding EF hands in the CaM N-lobe of the associated CaM provides an explanation. While both EF hands of the Ca^{2+}-loaded CaM N-lobe contain a sufficient number of acidic and polar residues (a total of five) positioned to coordinate Ca^{2+} in an optimal geometry (Fig. 4B and see Fig. 2D), the Na_V CTD EF hand does not (Fig. 4B). Thus, we conclude that the Na_V CTD EF hand does not likely bind Ca^{2+}; Ca^{2+}-dependent effects on Na_V channel function are more likely mediated via CaM.

Discussion

Whether and how Ca^{2+} contributes to the regulation of voltage-gated Na_V currents has been a focus of significant controversy since potential CaM binding sites were first identified within Na_V CTDs [5]. Our new structural model with Ca^{2+}/CaM bound to the $Na_V1.2$ CTD, in context with previous structures demonstrating the interaction of apoCaM with various Na_V CTDs [28, 29, 30], reveals novel and unexpected interactions between the Ca^{2+}-loaded CaM and the Na_V CTD. The apoCaM structures showed that the CaM C-lobe is anchored to the signature IQ motif within the extended IQ domain. On the basis of our new structural, biochemical, and functional data we propose that a major action of Ca^{2+} is to induce a conformational switch in the anchored CaM so that the CaM N-lobe swings into contact with the distal IQ domain while the Ca^{2+}-free CaM C-lobe remains anchored to the IQ motif (Fig. 2b). Interestingly, the new contact site for the calcified CaM N-lobe sits within a previously identified peptide that, when isolated from the adjacent IQ motif peptide, could only bind Ca^{2+}-loaded CaM, in contrast to the IQ motif that supported apoCaM binding over

Author Manuscript Author Manuscript Author Manuscript Author Manuscript

Ca^{2+}/CaM binding [5]. Additionally, we observed that Ca^{2+} induces rearrangements between the Na_V CTD and the CaM intralobular linker, and between the Na_V CTD and the CaM C-lobe (Fig. 3). We hypothesize that, together, these conformational changes may be propagated to the adjacent DIV transmembrane region of the channel to thereby affect Na_V function in an isoform-specific manner. Since our structures do not contain the transmembrane region of the channel, our model cannot explain how the conformational changes propagate to DIV. However, it is known that the conformational change of DIV voltage sensor (S4) is the rate-limiting step for channel inactivation [43, 44]. Thus, the Na_V CTD is in an advantageous position to affect channel gating.

Interestingly, the specific Ca^{2+}/CaM-dependent effects appear to vary among different Na_V channels [19]. Our data add to that concept in that we found that the wild type $Na_V1.2$ channel, not previously studied, was insensitive to Ca^{2+}/CaM for the parameters we studied at either nominally zero or saturating (~ 10 μM) intracellular Ca^{2+}. While the specific concentrations of internal Ca^{2+} studied here are outside the range of physiologic Ca^{2+} in neurons, these two levels allowed us to explore the bounds of Ca^{2+}, and correlate to our structures, obtained in the absence or presence of Ca^{2+}. These studies were also performed in the presence of a FHF, which was a component of the crystalized ternary complexes. Whether FHFs influence the Ca^{2+}-dependence of Na_V currents has not yet been analyzed. However, their inclusion in the functional studies is appropriate not only because of their presence in the crystal structures, but also because of growing evidence that FHFs are important regulators of Na_V currents in the neurons and cardiomyocytes [4, 16, 32, 45] in which $Na_V1.2$ and $Na_V1.5$ are expressed.

Nevertheless, the familial autism mutation Arg1902Cys introduced a large Ca^{2+}-dependent shift in both channel activation and steady-state inactivation (Fig. 3 and discussed below). A gain-of-function effect of a channelopathic mutation is reminiscent to the mechanism by which mutations in $Na_V1.5$ lead to Long QT Syndrome [9, 10] and in some $Na_V1.2$ mutations associated with epilepsy [46]. Combined with analysis of the $Na_V1.2/Ca^{2+}$ structure, our functional data suggests that the relayed interactions from Lys95 (CaM) through Glu1905 (Nav IQ domain) to Arg1902 (Nav globular domain) mask a Ca^{2+}-dependent shift in wild type $Na_V1.2$ that is revealed by the Arg1902Cys familial autism mutant when the relay is disrupted. It is noteworthy that an Asp96Val mutation adjacent to Lys95 in CaM, recently reported in a patient with an arrhythmia syndrome, was also associated with moderate cognitive impairment [14].

Taken together, we suggest that similar Ca^{2+}-induced conformational changes of CaM in both $Na_V1.2$ and $Na_V1.5$ (interactions of the CaM N-lobe to the distal IQ domain of Na_V CTD) might be responsible for Ca^{2+}-dependent regulation, and that their functional effects are isoform-specific. The concept that Ca^{2+}-dependent regulation may be isoform-specific is consistent with a recent report showing that a rapid increase in intracellular Ca^{2+} diminished transient Na_V currents through $Na_V1.4$, but not through the $Na_V1.5$ isoform [47]. With regard to $Na_V1.2$, only Arg1902Cys or Glu1905Gln unveiled a Ca^{2+}-dependent functional effect. We reasoned that there are possible reasons for these isoform-specific differences of Ca^{2+} dependence. First, in the context of the full-length channels, it is possible that the conformational changes at the CTD could propagate to the DIV transmembrane region of

Author Manuscript Author Manuscript Author Manuscript Author Manuscript

the channel differently depending on the isoforms. The apparent isoform-specific difference in the angle between the Na_V globular domain and the extended IQ domain reported herein (Fig. 1e) provide one possibility. For example, perhaps the difference in the angle within $Na_V1.2$ masks the Ca^{2+}-dependent changes in $Na_V1.2$ wild-type channel function initiated by the Ca^{2+}-dependent CaM N-lobe interaction. Second, it is possible that there are unexamined functional parameters that are more relevant to Ca^{2+}-dependent regulations that are less-isoform specific. Third, it is possible that Ca^{2+}/CaM does not mediate the observed Ca^{2+}-dependent changes in functions of $Na_V1.2$ Arg1902Cys or Glu1905Gln. However, the fact that Val1925Lys mutation (in the background of Arg1902Cys) abolishes the Ca^{2+}-dependent functional effect eliminates this possibility, as Val1925Lys would disrupt the binding of the CaM N-lobe to the distal IQ motif of $Na_V1.2$.

While mutagenesis studies have yielded suggestions about how Ca^{2+}/CaM regulates Na_V channel function [18, 19, 21, 38, 42, 48, 49], human disease mutations can be particularly revealing. By identifying new Ca^{2+}/CaM-dependent contacts with the Na_V CTD and demonstrating Ca^{2+}-dependent conformation changes within the complex, our data provide a context in which to consider the effects of disease mutations that affect Na_V CTD-CaM interaction. Several epilepsy mutations in $Na_V1.1$ or $Na_V1.2$ are in residues that make different contacts with Ca^{2+}/CaM compared to apoCaM (Fig. 3) as are additional $Na_V1.1$ and $Na_V1.2$ mutations associated with sporadic and familial cases of autism [7, 25, 26]. Further, our analysis of the effects of the $Na_V1.2$ Arg1902Cys familial autism mutation demonstrates that disruption of the wild type interaction between the CaM C-lobe and the CTD induces a Ca^{2+}-dependent change for the mutant $Na_V1.2$ channel function. The marked hyperpolarizing shift in both $Na_V1.2$ activation and inactivation induced by the Arg1902Cys autism mutation would affect neuronal excitability in $Na_V1.2$ expressing neurons, thus leading to an imbalance between excitation and inhibition known to drive neuropsychiatric phenotypes [50]. Additionally, our identification of the Ca^{2+}-dependent CaM N-lobe interaction with the distal IQ domain, not predicted by previous structural studies, provides a molecular mechanism for the Ca^{2+}-dependent dysfunction of the $Na_V1.5$ Ala1924Thr Brugada Syndrome mutation [20]. Finally, our data provide a potential mechanism for the recently described mutations in CaM associated with arrhythmias and cognitive deficits [14].

The Ca^{2+}-loaded ternary complexes present several unusual and novel features for a CaM-containing complex. Among these are the dissimilar conformations of the CaM N-lobe and CaM C-lobe when calcified CaM is bound to the IQ domain (Fig. 2C). While the different conformations of the individual CaM lobes in our structures mirror the CaM lobe conformations seen in the SK K^+ channel structure, the interactions between CaM and its target peptide(s) are markedly different. Within the SK K^+ channel homotetramer, the calcified CaM N-lobe wraps around one helix from the C-terminus of a protomer but the apoCaM C-lobe interacts with two helices from a different protomer within the tetramer [51]. Split roles for CaM lobes have also been suggested for Ca^{2+}-dependent regulation of Ca_V channels [52, 53, 54], with one lobe responsible for mediating changes to global Ca^{2+} while the other responds to changes in local Ca^{2+}. Comparison of our structures with Ca_V Ca^{2+} channel-derived structure provides an interesting contrast in structure and mechanisms by which Ca^{2+} regulates ion channel function, particularly since voltage-gated Na^+ channels and Ca^{2+} channels are similar in sequence within their proximal CTDs. The similarities

Author Manuscript Author Manuscript Author Manuscript Author Manuscript

include not only the IQ domain to which CaM binds but also an EF hand motif in the $Ca_V1.2$ L-type Ca^{2+} channel that was hypothesized to serve as a site for Ca^{2+}-dependent regulation [55], but (similar to the EF-hand in the Na_V CTD) has also never been shown to bind Ca^{2+} with a physiologically meaningful affinity. In spite of these similarities in sequence, structures of the Ca_V CTDs bound to CaM are surprisingly different from what we observe for the Na_V CTDs. Foremost among these differences is that the Ca_V CTD/CaM complexes crystallized as a dimer of CTDs, and each CTD interacted with two CaM molecules for an overall stoichiometry of 4 CaM and 2 CTDs [56, 57]. Whether the dimerization of channels observed in the structure is functionally relevant has been debated. Nevertheless, the 2:1 stoichiometry between CaM and the $Ca_V1.2$ CTD contrasts markedly with the 1:1 stoichiometry between CaM and a Na_V CTD. With these differences, it is not surprising that the overall fold of the $Ca_V1.2$ CTD does not resemble the Na_V CTDs.

Even focusing specifically on the interactions between Ca^{2+}/CaM and the respective IQ domains, the structures reveal stark differences (Fig. 5A-C). First, the arrangement of CaM with respect to the Na_V IQ domain is very different than Ca_V IQ domains. In both $Ca_V1.2$ and $Ca_V2.1$ IQ domains, CaM wraps around the IQ motif in a right-handed helical fashion, regardless of the relative orientation of the IQ motifs (parallel or antiparallel to CaM lobes). On the contrary, CaM wraps around the Na_V IQ domain in a left-handed helical fashion. Second, the overall Ca^{2+}/CaM footprint on the Na_V IQ domain is longer. The signature IQ motif in Ca_V channels forms a central anchor for Ca^{2+}/CaM interactions with both CaM lobes, while the IQ motif residues in the Na_V structures form contacts mostly with the CaM's Ca^{2+}-free C-lobe. Thus, the Ca^{2+}/CaM N-lobe is located further towards the C-terminus on the Na_V IQ domains compared to the Ca_V IQ domains. A search of the Dali database [58] suggesting that the CaM conformation in the $Na_V1.2/Ca^{2+}$ and $Na_V1.5/Ca^{2+}$ structures is novel.

Together with this novel interaction mode between CaM and the $Na_V1.2$ CTDs, our structural, biochemical, and functional data provide a new framework for understanding how CaM affects Na_V channels in physiology and disease.

Methods

Molecular biology

The following plasmids, for protein expression and purification, have been previously described: For crystallization the human $Na_V1.5$ CTD (amino acids 1773-1940) and $Na_V1.2$ (amino acids 1777-1937) were cloned into pET28 (Novagen) [21]; the human FGF13U (accession # NM_033642) and FGF12B were cloned into the second multiple cloning site of pETDuet-1 (Novagen) [59]; and CaM was cloned into pSGC02 [21]. For isothermal titration calorimetry, human $Na_V1.5$ CTD amino acids 1773-1924, $Na_V1.5$ CTD amino acids 1773-1940 (and the Ala1924Thr mutant) were cloned into pET28. For electrophysiology, $Na_V1.2$ was in pcDNA3.1 and FGF14b has previously been described [60]. Site-directed mutagenesis was performed with QuikChange (Stratagene).

Author Manuscript Author Manuscript Author Manuscript Author Manuscript

Recombinant protein expression and co-purification

The three plasmids for His6-Nav1.5 CTD, FGF12B, and CaM or His6-Nav1.2 CTD, FGF13U and CaM were co-electroporated into BL-21 (DE3) cells. Proteins were grown in LB medium or M9 medium as described [30]. Cells were harvested and resuspended in 300 mM NaCl, 20 mM Tris-HCl, 5 mM imidazole, 2 mM $CaCl_2$, pH 7.5, supplemented with EDTA-free protease inhibitor mixture (Roche). The initial purification protocol has been previously described [30]. Additional purification was performed by gel filtration on a Superdex 200 10/300L column on an AKTA FPLC (GE Healthcare) in 300 mM NaCl, 20mM Tris-HCl, 5 mM imidazole, with 2 mM $CaCl_2$, pH 7.5. Protein concentrations were determined by UV absorbance with Thermo NANODROP and were concentrated to A_{280} = 12 in above buffer for crystallization. For ITC experiments, the single plasmid was electroporated into BL-21 (DE3) cells and the proteins were expressed after induction with 1 mM isopropyl-1-thio-β-D-galactopyranoside (IPTG) for 16h at 20°C. CaM protein was purified as previously described [41].

Crystallization, data collection and structure determination

Crystals were grown by vapor diffusion with the sitting-drop method. His6-Nav1.5 CTD, FGF12B, and Ca^{2+}/CaM crystals were obtained with 20% PEG3350, 0.18 M $MgSO_4$, 0.1 M sodium iodide, and 2 mM $CaCl_2$. His6-Nav1.2 CTD, FGF13U, and CaM selenomethionine incorporated proteins crystals were obtained with 14% pEG3350, 300 mM sodium acetate, 50 mM Tris pH 7.5, and 2 mM $CaCl_2$. Before flash-freezing in liquid nitrogen, the crystals were cryoprotected by gradually increasing the concentration of glycerol in the well solution to 20%.

Crystals of selenomethionine (SeMet)-substituted $Na_V1.2$ in complex with Ca^{2+}/CaM and FGF13 diffract to 3.02 Å Bragg spacings with the space group C2 and crystals of human $Na_V1.5$ CTD in complex with Ca^{2+}/CaM and FGF12B diffract to 3.8 Å /5.4 Å /6 Å with the space group $P3_121$ (Table 1). As for the structure determination of the complex of $Na_V1.2$ CTD, Ca^{2+}-CaM, and FGF13U, experimental phases were obtained from the SeMet-substituted complex using single anomalous dispersion (SAD). After initial automatic model building, model building was completed manually. The final model contains two complexes in the asymmetric unit and is refined to R/R_{free} of 21.5/24.6% with good geometry (Table 1). The model contains residues 1788 to 1929 of Nav1.2. As for the structure determination of the complex of $Na_V1.5$, Ca^{2+}-CaM, and FGF12B, molecular replacement was performed to obtain the phases. In brief, the EF hand domain (residue 1786-1896) together with FGF13 from the previous Nav1.5 CTD structure in complex with FGF13U structure and Mg^{2+}-CaM (PDB ID:4DCK), IQ domain (residue 1899-1919) from the same complex structure, and the C-lobe of Mg^{2+}-CaM (residue 85-145) were used as independent search models and used to find the solutions using Phaser [61]. After the solution was found, the N-lobe of CaM was manually placed using F_o-F_c map. Low-resolution structure refinement was performed using the reference model as the complex of Nav1.2, Ca^{2+}/CaM and FGF13. The serious anisotropy of amplitudes were corrected using the UCLA Diffraction Anisotropy Server (http://services.mbi.ucla.edu/anisoscale) [62] and was used for the refinement. The final model contains one complex in the asymmetric unit and is of good quality with R/R_{free} of 26.0/31.8% (Table 1).

Author Manuscript Author Manuscript Author Manuscript Author Manuscript

Isothermal Titration Calorimetry

Experiments were performed with an ITC-200 (MicroCal) at 20 °C. The solutions containing the wild type $Na_V1.5$ CTD, $Na_V1.2$ CTD , $Na_V1.2$ CTD R1902C mutation, $Na_V1.5$ CTD amino acids 1773-1924, truncation mutant, or A1924T mutant (25-35 μM) were titrated with 1 injection of 5 μl and 27 injections of 10 μl of solutions containing CaM or CaM_{34} (240-310 μM). ITC experiments were repeated with different preparations and different concentrations at least three times to confirm thermodynamic parameters and stoichiometry values. The binding isotherms were analyzed with a single site binding model using the Microcal Origin version 7.0 software package (Originlab Corporation), yielding binding enthalpy (ΔH), stoichiometry (n), entropy (ΔS), and association constant (K_a). Results are presented as mean ± standard error; statistical significance was assessed using a two-tailed Student's *t*-test and was set at $P < 0.05$.

Electrophysiology

Human embryonic kidney (HEK) 293T cells (ATCC) were cultured in Dulbecco's modified Eagle's medium (DMEM) supplemented with 10% heat-inactivated fetal bovine serum (FBS). The cells were plated on 60-mm tissue culture dishes and grown to 65%–75% confluence, then transfected using Lipofectamine 2000 (Invitrogen) with a total 6 μg of cDNAs encoding $Na_V1.2$, FGF14b, β1, and β2 at a ratio of 2:1:1. One day after transfection, the cells were re-plated on coverslips coated with 50 μg/ml poly-D-lysine (Sigma) for electrophysiological recordings. Transfected cells were identified by GFP fluorescence. Na^+ currents were recorded using the whole-cell patch-clamp technique at room temperature (20-22 °C) 48-72 h after transfection. Electrode resistance ranged from 2.5-2.5 MΩ. Currents were filtered at 2.9 kHz and digitized at 20 Hz using an EPC 10 USB patch amplifier (HEKA Elektronik). Cells were allowed to stabilize for 7-10 min after the whole-cell configuration was established. Cells expressing peak currents amplitude >6000 pA were excluded from kinetic analyses because of suboptimal voltage control, as were cells exhibiting peak current amplitudes <600 pA to avoid contamination by endogenous currents. All cells were included in analyses of current density. The liquid junction potential, series resistance and leak current for these recordings were not corrected, and cells were discarded if series resistance was >8 MΩ. The bath solution contained (in mM): NaCl 124, TEA-Cl 20, $CaCl_2$ 2.0, $MgCl_2$ 1, HEPES 5, glucose 10, pH 7.3 (adjusted with NaOH). The intracellular "0 Ca^{2+}" solution contained (in mM): $CsCl_2$ 60, L-aspartic acid 80, 1,2-bis(o-amino phenoxy)ethane-N,N,N′,N′-tetraacetic acid (BAPTA) 10, HEPES 10, pH 7.35 (adjusted with CsOH). The intracellular "10 μM Ca^{2+}" solution contained (in mM): $CsCl_2$ 60, L-aspartic acid 80, BAPTA 1, $CaCl_2$ 1, HEPES 10, pH 7.30 (adjusted with CsOH). Osmolarity was adjusted to 310 mOsm with sucrose for all solutions. The voltage-clamp protocols were generated by PatchMaster. Cells were voltage-clamped at a holding potential (V_h) of -120 mV, and currents were elicited by depolarizing pulses of 40 ms from -120 mV to +45 mV in 5 mV increments. Current density was calculated by normalizing to cell capacitance. Activation curves were obtained by transforming current data to conductance (G), which was calculated from the equation $G_{Na} = I/(V - E_{rev})$, where: I is the peak Na^+ current elicited by the depolarizing test potential; V is the test potential; and E_{rev} is the calculated Na^+ reversal potential. The ratio G/G_{max} was plotted against the membrane potential and fitted

Author Manuscript Author Manuscript Author Manuscript Author Manuscript

with the Boltzmann equation of the form: $G / G_{max}=(1+\exp[(V-V_{1/2})/k])^{-1}$, where Gmax is the extrapolated maximum conductance, V is the test voltage, $V_{1/2}$ is the half-activation voltage, and *k* is the slope factor. Standard two-pulse protocols were used to generate the steady-state inactivation curves: from a holding potential of -120 mV, cells were stepped to 500-ms preconditioning potentials varying between -130 mV and -10 mV (prepulse) in 5 mV increments, followed by a 20 ms test pulse to -20 mV. Currents (*I*) were normalized to I_{max} and fit to a Boltzmann function of the form I/Imax =1/(1+exp((Vm-V1/2)/k)) in which $V_{1/2}$ is the voltage at which half of $Na_V1.5$ channels are inactivated, *k* is the slope factor and V_m is the membrane potential. Data analysis was performed using FitMaster (HEKA Elektronik) and Origin 8 software. Results are presented as means ± standard error; the statistical significance of differences between groups was assessed using a two-tailed Student's *t*-test and was set at $P< 0.05$.

Supplementary Material

Refer to Web version on PubMed Central for supplementary material.

Acknowledgments

Data for this study were collected at beam lines NE-CAT ID 24-C and SER-CAT BM22/ID22 and at the Advanced Photon Source and the Duke X-ray Crystallography Facility. We thank R. Brennan, M. Schumacher, and P. Zhou for providing access to their ITC machines; C. Pemble for help with remote data collection. This work was supported by NHLBI R01 HL71165 and HL113136 (G.S.P.), and American Heart Association Established Investigator Award (G.S.P.); start-up funds from the Duke University Medical Center (S.-Y.L.), the Basil O'Connor Starter Scholar Research Award 5-FY10-473 from the March of Dimes foundation (S.-Y.L.), the N.I.H. Director's New Innovator Award 1 DP2 OD008380-01 (S.-Y.L). S.-Y.L. is a McKnight Scholar, Klingenstein fellow, Alfred P. Sloan Research fellow, Mallinckrodt Scholar, and Whitehead Scholar. The funders had no role in study design, data collection and analysis, decision to publish, or preparation of the manuscript.

References

1. Payandeh J, Scheuer T, Zheng N, Catterall WA. The crystal structure of a voltage-gated sodium channel. Nature. 2011; 475:353–358. [PubMed: 21743477]
2. Payandeh J, Gamal El-Din TM, Scheuer T, Zheng N, Catterall WA. Crystal structure of a voltage-gated sodium channel in two potentially inactivated states. Nature. 2012; 486:135–139. [PubMed: 22678296]
3. Mantegazza M, Yu FH, Catterall WA, Scheuer T. Role of the C-terminal domain in inactivation of brain and cardiac sodium channels. Proc Natl Acad Sci U S A. 2001; 98:15348–15353. [PubMed: 11742069]
4. Goldfarb M, et al. Fibroblast growth factor homologous factors control neuronal excitability through modulation of voltage-gated sodium channels. Neuron. 2007; 55:449–463. [PubMed: 17678857]
5. Mori M, Konno T, Ozawa T, Murata M, Imoto K, Nagayama K. Novel interaction of the voltage-dependent sodium channel (VDSC) with calmodulin: does VDSC acquire calmodulin-mediated Ca2+-sensitivity? Biochemistry. 2000; 39:1316–1323. [PubMed: 10684611]
6. Catterall WA, Kalume F, Oakley JC. NaV1.1 channels and epilepsy. J Physiol. 2010; 588:1849–1859. [PubMed: 20194124]
7. Weiss LA, et al. Sodium channels SCN1A, SCN2A and SCN3A in familial autism. Mol Psychiatry. 2003; 8:186–194. [PubMed: 12610651]
8. Lossin C. A catalog of SCN1A variants. Brain & development. 2009; 31:114–130. [PubMed: 18804930]
9. Wang Q, et al. SCN5A mutations associated with an inherited cardiac arrhythmia, long QT syndrome. Cell. 1995; 80:805–811. [PubMed: 7889574]

Author Manuscript Author Manuscript Author Manuscript Author Manuscript

10. Bennett PB, Yazawa K, Makita N, George AL Jr. Molecular mechanism for an inherited cardiac arrhythmia. Nature. 1995; 376:683–685. [PubMed: 7651517]
11. Antzelevitch C. Brugada syndrome: report of the second consensus conference: endorsed by the Heart Rhythm Society and the European Heart Rhythm Association. Circulation. 2005; 111:659–670. [PubMed: 15655131]
12. Bannister RA, Melliti K, Adams BA. Differential modulation of CaV2.3 Ca2+ channels by Galphaq/11-coupled muscarinic receptors. Mol Pharmacol. 2004; 65:381–388. [PubMed: 14742680]
13. Bezzina CR, et al. Compound heterozygosity for mutations (W156X and R225W) in SCN5A associated with severe cardiac conduction disturbances and degenerative changes in the conduction system. Circ Res. 2003; 92:159–168. [PubMed: 12574143]
14. Crotti L, et al. Calmodulin mutations associated with recurrent cardiac arrest in infants. Circulation. 2013; 127:1009–1017. [PubMed: 23388215]
15. van Swieten JC, et al. A Mutation in the Fibroblast Growth Factor 14 Gene Is Associated with Autosomal Dominant Cerebral Ataxia. The American Journal of Human Genetics. 2003; 72:191–199. [PubMed: 12489043]
16. Hennessey JA, et al. FGF12 is a candidate Brugada syndrome locus. Heart Rhythm. 2013; 10:1886–1894. [PubMed: 24096171]
17. Pitt GS. Calmodulin and CaMKII as molecular switches for cardiac ion channels. Cardiovasc Res. 2007; 73:641–647. [PubMed: 17137569]
18. Wingo TL, Shah VN, Anderson ME, Lybrand TP, Chazin WJ, Balser JR. An EF-hand in the sodium channel couples intracellular calcium to cardiac excitability. Nat Struct Mol Biol. 2004; 11:219–225. [PubMed: 14981509]
19. Herzog RI, Liu C, Waxman SG, Cummins TR. Calmodulin binds to the C terminus of sodium channels Nav1.4 and Nav1.6 and differentially modulates their functional properties. J Neurosci. 2003; 23:8261–8270. [PubMed: 12967988]
20. Tan HL, et al. A calcium sensor in the sodium channel modulates cardiac excitability. Nature. 2002; 415:442–447. [PubMed: 11807557]
21. Kim J, Ghosh S, Liu H, Tateyama M, Kass RS, Pitt GS. Calmodulin mediates Ca2+ sensitivity of sodium channels. J Biol Chem. 2004; 279:45004–45012. [PubMed: 15316014]
22. Rusconi R, et al. A rescuable folding defective Nav1.1 (SCN1A) sodium channel mutant causes GEFS+: common mechanism in Nav1.1 related epilepsies? Hum Mutat. 2009; 30:E747–760. [PubMed: 19402159]
23. Haug K, et al. The voltage-gated sodium channel gene SCN2A and idiopathic generalized epilepsy. Epilepsy Res. 2001; 47:243–246. [PubMed: 11738931]
24. Zucca C, et al. Cryptogenic epileptic syndromes related to SCN1A: twelve novel mutations identified. Arch Neurol. 2008; 65:489–494. [PubMed: 18413471]
25. Sanders SJ, et al. De novo mutations revealed by whole-exome sequencing are strongly associated with autism. Nature. 2012; 485:237–241. [PubMed: 22495306]
26. O'Roak BJ, et al. Sporadic autism exomes reveal a highly interconnected protein network of de novo mutations. Nature. 2012; 485:246–250. [PubMed: 22495309]
27. O'Roak BJ, et al. Exome sequencing in sporadic autism spectrum disorders identifies severe de novo mutations. Nat Genet. 2011; 43:585–589. [PubMed: 21572417]
28. Feldkamp MD, Yu L, Shea MA. Structural and energetic determinants of apo calmodulin binding to the IQ motif of the Na(V)1.2 voltage-dependent sodium channel. Structure. 2011; 19:733–747. [PubMed: 21439835]
29. Chagot B, Chazin WJ. Solution NMR structure of Apo-calmodulin in complex with the IQ motif of human cardiac sodium channel NaV1.5. J Mol Biol. 2011; 406:106–119. [PubMed: 21167176]
30. Wang C, Chung BC, Yan H, Lee SY, Pitt GS. Crystal structure of the ternary complex of a NaV C-terminal domain, a fibroblast growth factor homologous factor, and calmodulin. Structure. 2012; 20:1167–1176. [PubMed: 22705208]
31. Laezza F, et al. The FGF14(F145S) mutation disrupts the interaction of FGF14 with voltage-gated Na+ channels and impairs neuronal excitability. J Neurosci. 2007; 27:12033–12044. [PubMed: 17978045]

Author Manuscript Author Manuscript Author Manuscript Author Manuscript

32. Wang C, et al. Fibroblast growth factor homologous factor 13 regulates Na+ channels and conduction velocity in murine hearts. Circ Res. 2011; 109:775–782. [PubMed: 21817159]
33. Miloushev VZ, Levine JA, Arbing MA, Hunt JF, Pitt GS, Palmer AG 3rd. Solution structure of the NaV1.2 C-terminal EF-hand domain. J Biol Chem. 2009; 284:6446–6454. [PubMed: 19129176]
34. Chagot B, Potet F, Balser JR, Chazin WJ. Solution NMR structure of the C-terminal EF-hand domain of human cardiac sodium channel NaV1.5. J Biol Chem. 2009; 284:6436–6445. [PubMed: 19074138]
35. Goetz R, et al. Crystal structure of a fibroblast growth factor homologous factor (FHF) defines a conserved surface on FHFs for binding and modulation of voltage-gated sodium channels. J Biol Chem. 2009; 284:17883–17896. [PubMed: 19406745]
36. Houdusse A, Cohen C. Target sequence recognition by the calmodulin superfamily: implications from light chain binding to the regulatory domain of scallop myosin. Proc Natl Acad Sci U S A. 1995; 92:10644–10647. [PubMed: 7479857]
37. Meador WE, Means AR, Quiocho FA. Target enzyme recognition by calmodulin: 2.4 A structure of a calmodulin-peptide complex. Science. 1992; 257:1251–1255. [PubMed: 1519061]
38. Sarhan MF, Tung CC, Van Petegem F, Ahern CA. Crystallographic basis for calcium regulation of sodium channels. Proc Natl Acad Sci U S A. 2012; 109:3558–3563. [PubMed: 22331908]
39. Willsey AJ, et al. Coexpression networks implicate human midfetal deep cortical projection neurons in the pathogenesis of autism. Cell. 2013; 155:997–1007. [PubMed: 24267886]
40. Wang Q, et al. Ataxia and paroxysmal dyskinesia in mice lacking axonally transported FGF14. Neuron. 2002; 35:25–38. [PubMed: 12123606]
41. Wang C, Wang HG, Xie H, Pitt GS. Ca2+/CaM controls Ca2+-dependent inactivation of NMDA receptors by dimerizing the NR1 C termini. J Neurosci. 2008; 28:1865–1870. [PubMed: 18287503]
42. Shah VN, Wingo TL, Weiss KL, Williams CK, Balser JR, Chazin WJ. Calcium-dependent regulation of the voltage-gated sodium channel hH1: intrinsic and extrinsic sensors use a common molecular switch. Proc Natl Acad Sci U S A. 2006; 103:3592–3597. [PubMed: 16505387]
43. Cha A, Ruben PC, George AL, Fujimoto E, Bezanilla F. Voltage Sensors in Domains III and IV, but Not I and II, Are Immobilized by Na+ Channel Fast Inactivation. Neuron. 1999; 22:73–87. [PubMed: 10027291]
44. Capes DL, Goldschen-Ohm MP, Arcisio-Miranda M, Bezanilla F, Chanda B. Domain IV voltage-sensor movement is both sufficient and rate limiting for fast inactivation in sodium channels. J Gen Physiol. 2013; 142:101–112. [PubMed: 23858005]
45. Shakkottai VG, et al. FGF14 regulates the intrinsic excitability of cerebellar Purkinje neurons. Neurobiol Dis. 2009; 33:81–88. [PubMed: 18930825]
46. Meisler MH, Kearney JA. Sodium channel mutations in epilepsy and other neurological disorders. J Clin Invest. 2005; 115:2010–2017. [PubMed: 16075041]
47. Ben-Johny M, Yang PS, Niu J, Yang W, Joshi-Mukherjee R, Yue DT. Conservation of Ca/Calmodulin Regulation across Na and Ca Channels. Cell. 2014; 157:1657–1670. [PubMed: 24949975]
48. Potet F, et al. Functional Interactions between Distinct Sodium Channel Cytoplasmic Domains through the Action of Calmodulin. J Biol Chem. 2009; 284:8846–8854. [PubMed: 19171938]
49. Sarhan MF, Van Petegem F, Ahern CA. A double tyrosine motif in the cardiac sodium channel domain III-IV linker couples calcium-dependent calmodulin binding to inactivation gating. J Biol Chem. 2009; 284:33265–33274. [PubMed: 19808664]
50. Yizhar O, et al. Neocortical excitation/inhibition balance in information processing and social dysfunction. Nature. 2011; 477:171–178. [PubMed: 21796121]
51. Schumacher MA, Rivard AF, Bachinger HP, Adelman JP. Structure of the gating domain of a Ca2+-activated K+ channel complexed with Ca2+/calmodulin. Nature. 2001; 410:1120–1124. [PubMed: 11323678]
52. Erickson MG, Alseikhan BA, Peterson BZ, Yue DT. Preassociation of calmodulin with voltage-gated Ca(2+) channels revealed by FRET in single living cells. Neuron. 2001; 31:973–985. [PubMed: 11580897]

Author Manuscript Author Manuscript Author Manuscript Author Manuscript

53. Tadross MR, Dick IE, Yue DT. Mechanism of local and global Ca2+ sensing by calmodulin in complex with a Ca2+ channel. Cell. 2008; 133:1228–1240. [PubMed: 18585356]

54. DeMaria CD, Soong TW, Alseikhan BA, Alvania RS, Yue DT. Calmodulin bifurcates the local Ca2+ signal that modulates P/Q-type Ca2+ channels. Nature. 2001; 411:484–489. [PubMed: 11373682]

55. de Leon M, et al. Essential Ca(2+)-binding motif for Ca(2+)-sensitive inactivation of L-type Ca2+ channels. Science. 1995; 270:1502–1506. [PubMed: 7491499]

56. Kim EY, et al. Multiple C-terminal tail Ca(2+)/CaMs regulate Ca(V)1.2 function but do not mediate channel dimerization. EMBO J. 2010; 29:3924–3938. [PubMed: 20953164]

57. Fallon JL, et al. Crystal structure of dimeric cardiac L-type calcium channel regulatory domains bridged by Ca2+* calmodulins. Proc Natl Acad Sci U S A. 2009; 106:5135–5140. [PubMed: 19279214]

58. Holm L, Rosenstrom P. Dali server: conservation mapping in 3D. Nucleic Acids Res. 2010; 38:W545–549. [PubMed: 20457744]

59. Wang C, Wang C, Hoch EG, Pitt GS. Identification of novel interaction sites that determine specificity between fibroblast growth factor homologous factors and voltage-gated sodium channels. J Biol Chem. 2011; 286:24253–24263. [PubMed: 21566136]

60. Yan H, Pablo JL, Pitt GS. FGF14 regulates presynaptic Ca2+ channels and synaptic transmission. Cell Rep. 2013; 4:66–75. [PubMed: 23831029]

61. Adams PD, et al. PHENIX: a comprehensive Python-based system for macromolecular structure solution. Acta crystallographica Section D, Biological crystallography. 2010; 66:213–221.

62. Strong M, Sawaya MR, Wang S, Phillips M, Cascio D, Eisenberg D. Toward the structural genomics of complexes: crystal structure of a PE/PPE protein complex from Mycobacterium tuberculosis. Proc Natl Acad Sci U S A. 2006; 103:8060–8065. [PubMed: 16690741]

Author Manuscript Author Manuscript Author Manuscript Author Manuscript

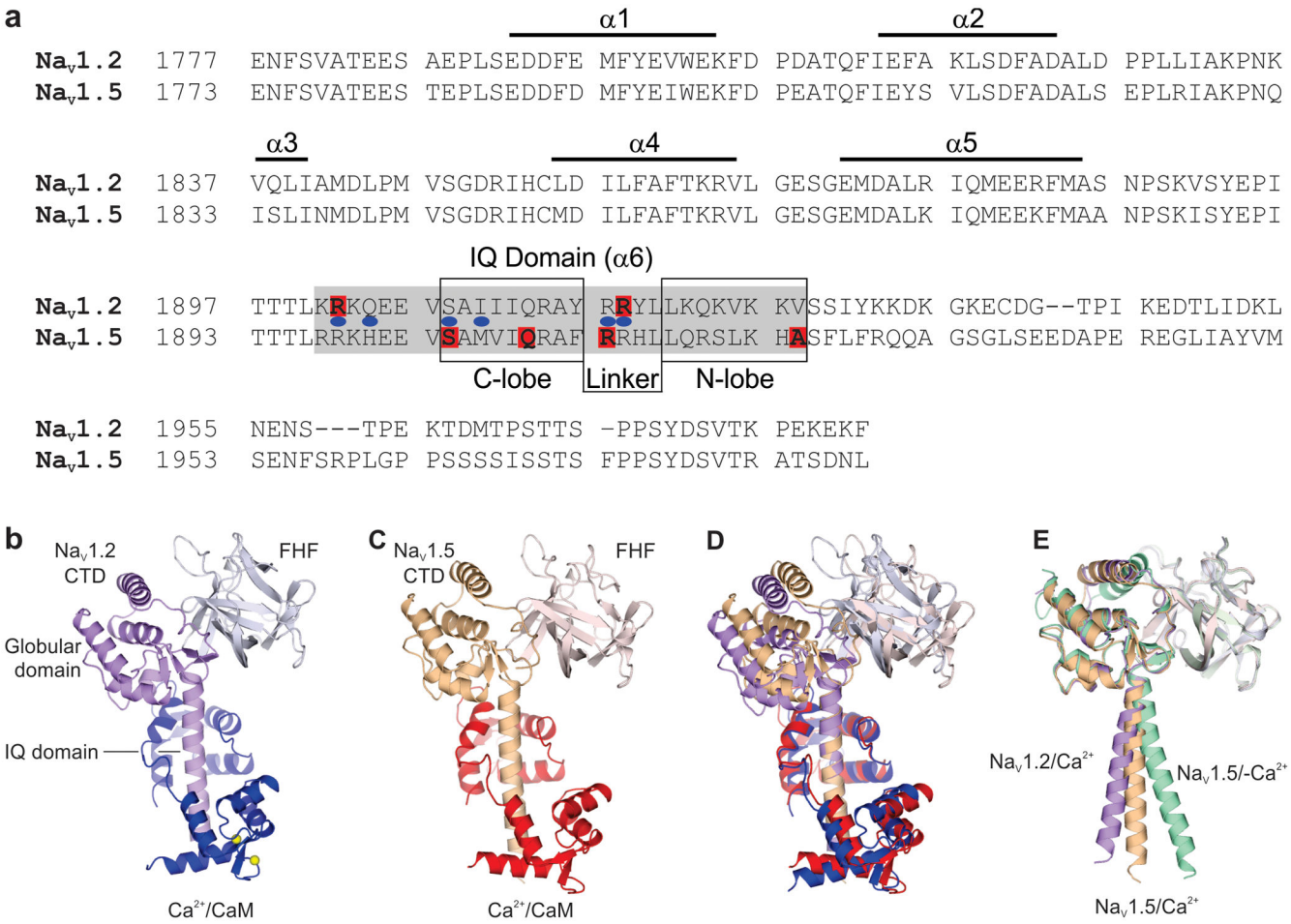

Figure 1. Overall architecture of the ternary complexes containing a Na$_V$ CTD, CaM, and a FHF

(**A**) Sequence alignment of the Na$_V$1.2 and Na$_V$1.5 CTDs, with structural motifs and the IQ domain indicated. The interaction sites for the CaM N- and C-lobes and the CaM interlobular linker are also indicated. Human disease mutations in Na$_V$1.2 and Na$_V$1.5 clustering in the IQ domain are indicated in red; in blue are the homologous positions of disease mutations in Na$_V$1.1. (**B**) The Na$_V$1.2/Ca^{2+} structure containing the Na$_V$1.2 CTD (purple), FGF13 (silver), and CaM (blue). (**C**) The Na$_V$1.5/Ca^{2+} structure containing the Na$_V$1.5 CTD (orange), FGF12 (pink), and CaM (red). (**D**) Overlay of the Na$_V$1.2/Ca^{2+} and the Na$_V$1.5/Ca^{2+} structures aligned to the IQ motifs. (**E**) Overlay of the Na$_V$1.2/Ca^{2+} structure; the Na$_V$1.5/Ca^{2+} structure; and the Na$_V$1.5/-Ca^{2+} structure (Protein Data Bank accession code 4DCK), all aligned to the globular domain of the respective CTDs. For clarity, their respective CaM structures were omitted. This arrangement emphasizes the different angles between the globular domains and the IQ motifs among the three structures.

Author Manuscript Author Manuscript Author Manuscript Author Manuscript

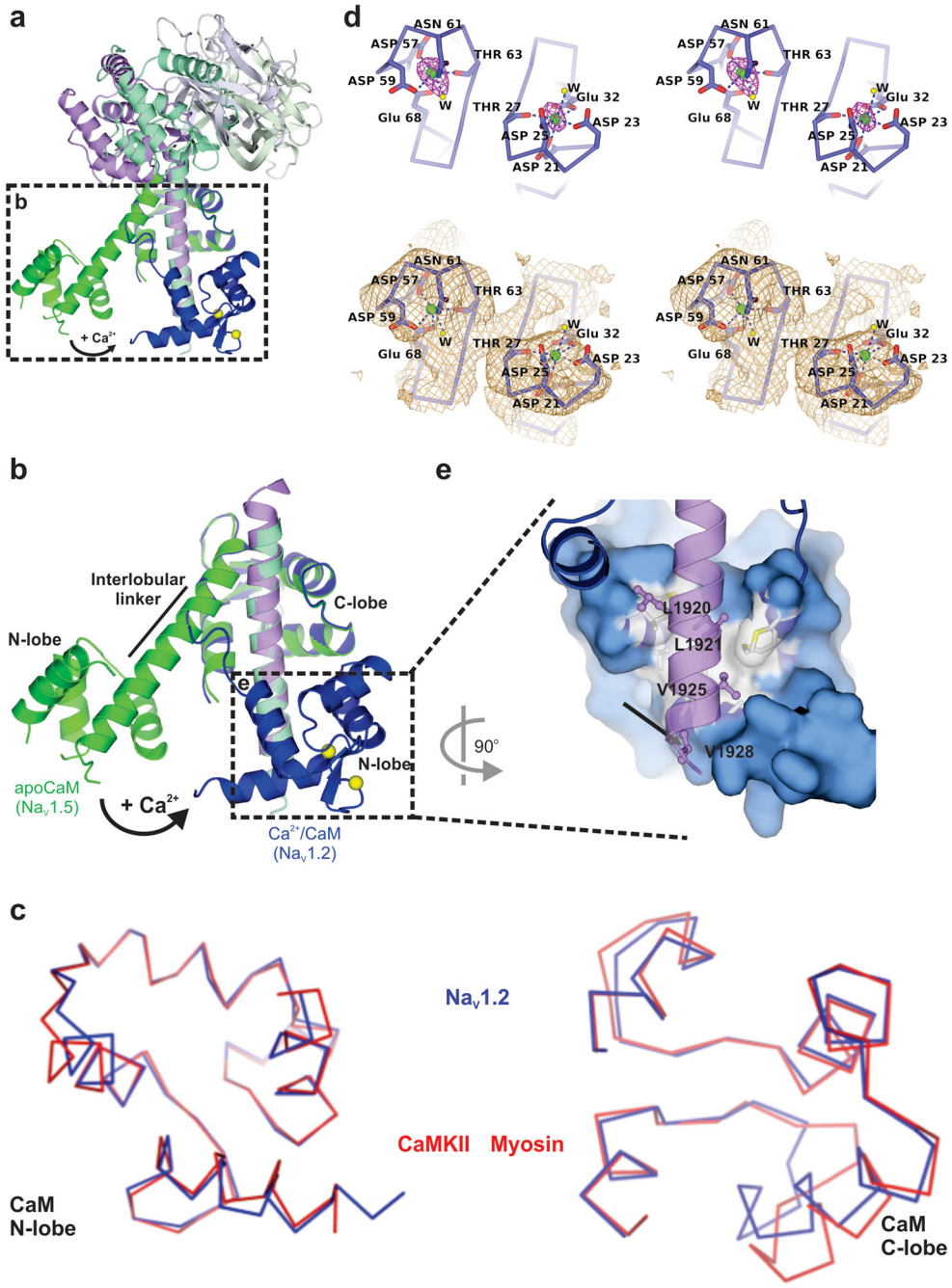

Figure 2. Ca^{2+}-dependent calmodulin interactions

(**A**) Overlay of the $Na_V1.2/Ca^{2+}$ and the $Na_V1.5/-Ca^{2+}$ structures, both aligned to their IQ domains. Colors for $Na_V1.2$: $Na_V1.2$ CTD (purple), FGF13 (silver), and CaM (blue). Colors for $Na_V1.5$: $Na_V1.5$ CTD (pale green), CaM (dark green), FGF12 (lime). (**B**) Zoomed-in view of the IQ domains and CaM with the same orientation as (**A**). Ca^{2+} ions are shown as yellow balls. Mg^{2+}-CaM from the $Na_V1.5/-Ca^{2+}$ structure is colored green and Ca^{2+}-CaM from the $Na_V1.2/Ca^{2+}$ structure is colored blue. (**C**) C α trace overlay of the Ca^{2+}-loaded CaM N-lobes (left) from the $Na_V1.2/Ca^{2+}$ structure (blue); and Ca^{2+}/CaM bound to the CaM

Author Manuscript Author Manuscript Author Manuscript Author Manuscript

binding peptide in CaMKII (PDB ID 3GP2, red); and the Ca^{2+}-free CaM C-lobes (right) from the $Na_V1.2/Ca^{2+}$ structure (blue); and CaM bound to the IQ motif in scallop myosin (PDB ID 2IX7, red). (**D**) Stereo view of the coordination geometry of the two Ca^{2+} binding sites in the CaM N-lobe within the $Na_V1.2/Ca^{2+}$ structure (top) with the Fo-Fc omit map for Ca^{2+} ions (magenta, 6 σ) and 2Fo-Fc omit map (bottom, salmon, 1σ). W stands for the water. (**E**) Zoomed-in view of the CaM/N-lobe (blue) interactions with $Na_V1.2/Ca^{2+}$ (purple).

Author Manuscript Author Manuscript Author Manuscript Author Manuscript

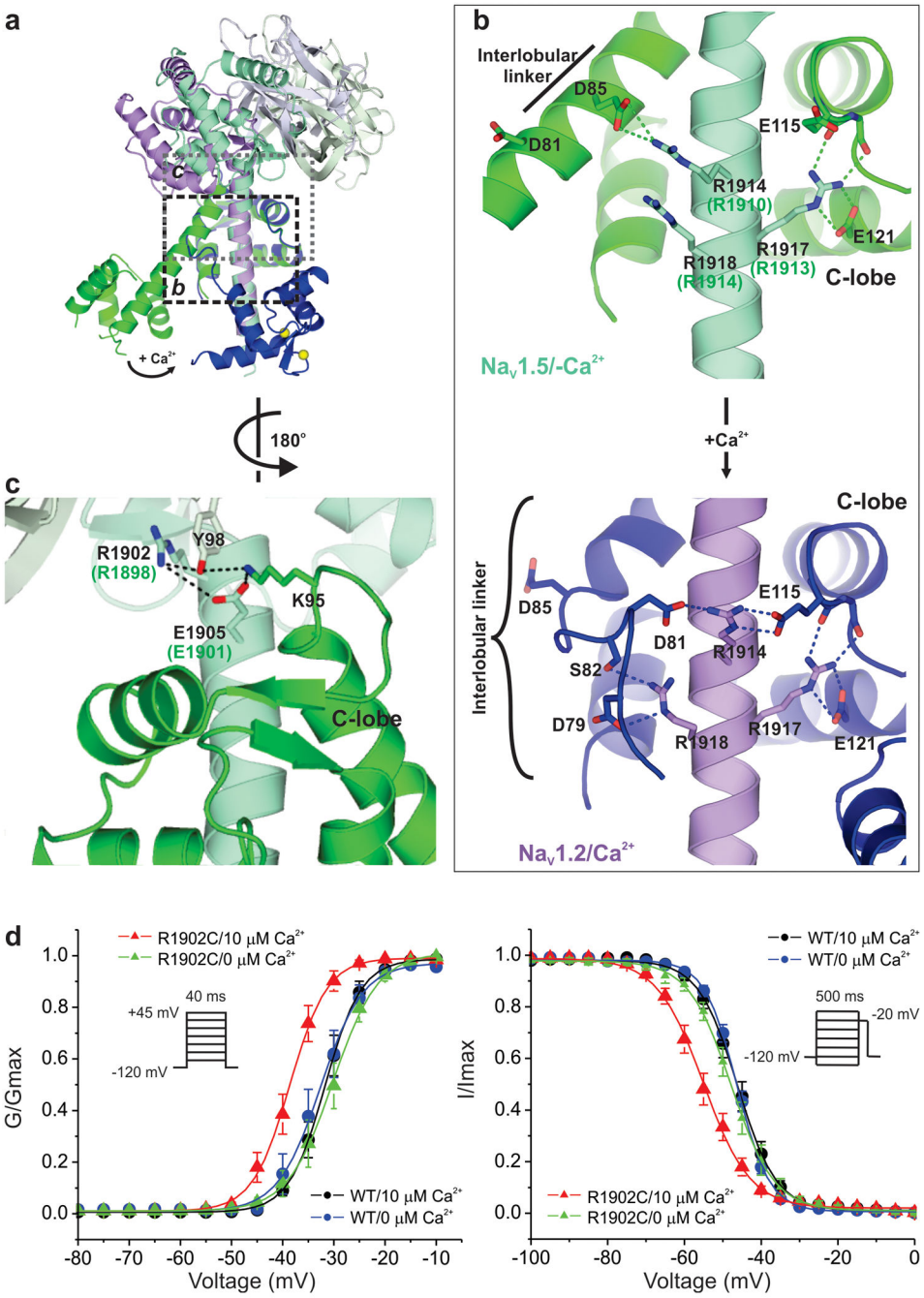

Figure 3. Ca^{2+}-dependent structural changes highlight mechanisms for Na_V channel dysfunction with disease mutations

(**A**) Overall structure of the $Na_V1.2/Ca^{2+}$ and $Na_V1.5/-Ca^{2+}$ complexes for orientation, as in Figure 2A. Boxed area shows the relative region for focus in **B** and **C**. (**B**) Zoomed view of the $Na_V1.5/-Ca^{2+}$ and $Na_V1.2/Ca^{2+}$ structures demonstrating the Ca^{2+}-dependent changes in interaction between the Na_V CTD and the CaM C-lobe and CaM interlobular linker. For comparison, the labeling for the Arg residues within the $Na_V1.5$ CTD employs the corresponding numbers for $Na_V1.2$; and the $Na_V1.5$ numbers are shown in parentheses. **C**)

Author Manuscript Author Manuscript Author Manuscript Author Manuscript

Zoomed view of the $Na_V1.5$/-Ca^{2+} structure focusing on the interaction between Arg1898 (Arg1902 in $Na_V1.2$) in the $Na_V1.5$ CTD and Lys95 in CaM via Glu1901 (Glu1905 in $Na_V1.2$) and Tyr98 in FGF13. As in **B**, the numbering within the CTD corresponds to the $Na_V1.2$ sequence and the $Na_V1.5$ equivalents are in parentheses. (**D**) Activation and steady-state inactivation relationships in 0 mM Ca^{2+} or 10 μM free Ca^{2+} in the recording pipette for wild type $Na_V1.2$ or the Arg1902Cys CaM N-lobe interaction mutant. Summary data and statistics are provided inTable 1.

Author Manuscript Author Manuscript Author Manuscript Author Manuscript

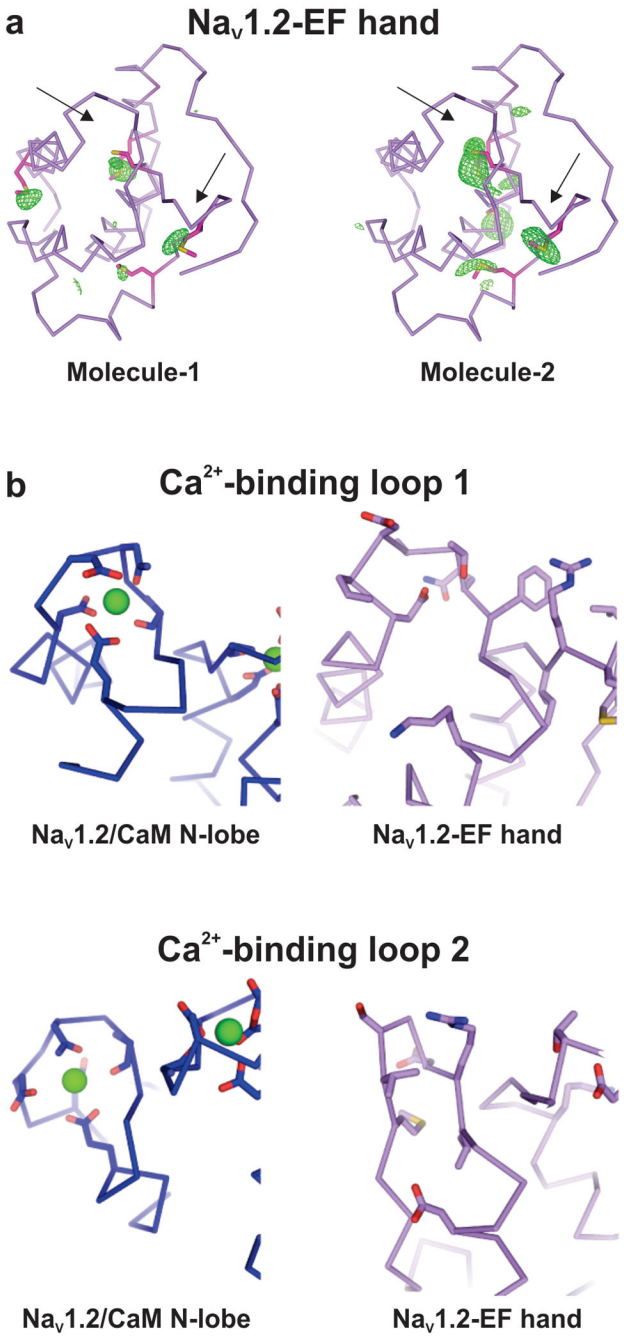

Figure 4. The Na$_V$ CTD EF hand does not bind Ca^{2+}

(**A**) Anomalous difference Fourier map for two CaMs in the asymmetric unit from the Na$_V$1.2 CTD crystal. The map was calculated using data from 25.0 Å- 5.5 Å of the native crystal using the final model phases. The anomalous difference peaks, colored in green mesh, are contoured at 2.8 σ. The arrows indicate the expected positions of Ca^{2+} in CaM. Side-chains of methionines are shown. (**B**) Comparison of the first and second Ca^{2+} binding loop in the CaM/N-lobe with the EF hand motif from the Na$_V$1.2 CTD. Side chains involved

in Ca^{2+} coordination in the Ca^{2+}-binding loops of EF hands are shown. Ca^{2+} is shown as a green ball.

Author Manuscript Author Manuscript Author Manuscript Author Manuscript

Author Manuscript Author Manuscript Author Manuscript Author Manuscript

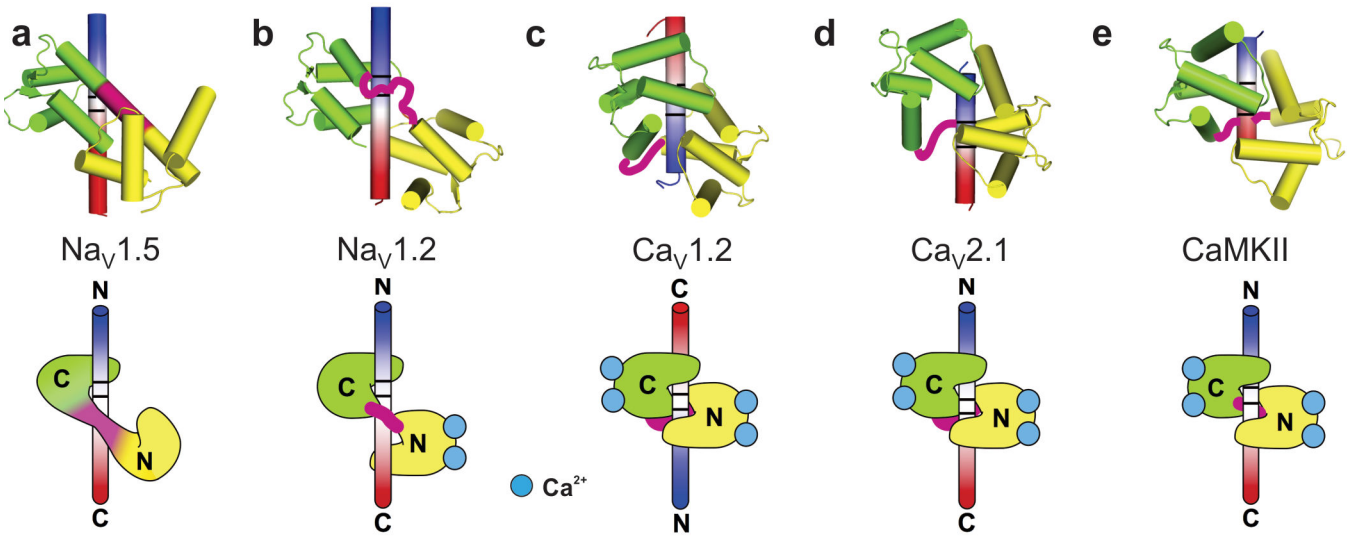

Figure 5. CaM conformations when bound to Na_V channels compared to Ca_V channels and CaMKII

(**A-E**) Unique arrangement of CaM relative to the IQ domains in the $Na_V1.5$/-Ca^{2+} structure (**A**), the $Na_V1.2$/Ca^{2+} structure (**B**); a $Ca_V1.2$ structure (**C**, PDB ID: 2BE6); a $Ca_V2.1$ structure (**D**, PDB ID: 3DVM) and autoinhibitory (CaM binding) peptide in CaMKII (**E**, PDB ID: 1CDM). CaM N-lobe and C-lobe are colored yellow and green, respectively and the orientation of IQ motifs or autoinhibitory peptide is indicated with a color gradient (N-terminus blue and C-terminus red). The positions of IQ(M) amino acid residues on the IQ domains or the ^{302}AI^{303} amino acid residues in the CaMKII autoinhibitory peptide are demarcated with two black lines. The cartoon figures are shown below each structure to illustrate the difference of the CaM-Nav1.2 interactions. CaM wraps around the Na_V IQ domains in the left-handed fashion in contrast to the right-handed wrapping seen in Ca_V structures and in CaMKII.

Author Manuscript Author Manuscript Author Manuscript Author Manuscript

Table 1

Data Collection, Phasing, and Refinement Statistics.

Data collection	SeMet Nav1.2/CaM/FGF13/Ca^{2+}	Nav1.5/CaM/FGF12B/Ca^{2+}	Nav1.5/CaM/FGF12B/Ca^{2+} with 6 Å cutoff
Space group	C2	$P3_121$	$P3_121$
Wavelength (Å)	0.9792	1.0	1.0
Cell dimensions			
a, *b*, *c* (Å)	153.13, 86.11, 109.40	115.199, 115.199, 120.107	115.199, 115.199, 120.107
α, β, γ (°)	90.0, 100.9, 90.0	90.0, 90.0, 120.0	90.0, 90.0, 120.0
Resolution (Å)	50.00 – 3.02 (3.07 – 3.02)	50.00 – 3.80 (3.87 – 3.80)*	50.00 – 6.00 (6.10 – 6.00)
R_{sym} (%)	16.4 (48.3)	6.9 (39.2)	5.7 (24.1)
I/σI	16.8 (1.5)	34.7 (1.8)	53.0 (7.6)
Completeness (%)	94.3 (66.6)	46.1 (13.2)	92.6 (61.5)
Redundancy	12.5 (5.6)	7.2 (2.2)	8.5 (6.5)
SAD Phasing			
Figure of Merit	0.30 (50.0 – 3.02 Å)		
Refinement			
Resolution (Å)	48.23– 3.02 (3.09 – 3.02)	41.75 – 3.84 (5.00 – 3.54)**	41.75 – 6.00 (7.00 – 6.00)
Completeness (%)	91.8 (53.0)	40.53 (12.91)	92.89 (81.72)
No. of reflections	26179	3700	2301
$R_{work/free}$	21.48 / 24.64	26.01 / 31.75	23.61 / 31.82
Ramachandran (%)			
Favored	95.7	95.5	95.5
Outliers	0.4	0.5	0.5
R.m.s.d			
Bond lengths (Å)	0.011	0.011	0.012
Bond angles (°)	1.04	0.996	1.093

$R_{sym} = \Sigma | Ii - < Ii > | / \Sigma Ii$, where < Ii > is the average intensity of symmetry-equivalent reflections. $R_{work} = \Sigma | F_o - F_c | / \Sigma | F_o |$, where F_o and F_c are the observed and calculated structure factors, respectively. R_{free} = R-factor calculated using a subset (5-8%) of reflection data chosen randomly and omitted throughout refinement. The figure of merit = $|F(hkl)_{best}|/|F(hkl)|$ and calculated using Phaser before density modification.

*The crystal diffracts anisotropically to 3.8/5.4/6.0 Å.

**The data treated with ellipsoidal truncation and anisotropic scaling was used for refinement(1).

Author Manuscript Author Manuscript Author Manuscript Author Manuscript

Table 2

Thermodynamic parameters for CaM interaction with the $Na_V1.5$ CTD

Titrant	*N*	Cell	K_d (nM)	ΔH (kcal/mol)	ΔS(cal·mol^{-1}· deg^{-1})	N value
Ca^{2+}/CaM	3	1773-1924	1990 ± 358 *	-3.77 ± 0.27	12.4 ± 0.5	0.38 ± 0.02
apoCaM	4	1773-1940	88 ± 6 *	-10.69 ± 0.06	-4.2 ± 0.3	0.94 ± 0.03
Ca^{2+}/CaM	3	1773-1940	132 ± 9	-9.94 ± 0.33	-2.4 ± 0.1	0.83 ± 0.05
Ca^{2+}/CaM	3	1773-1940 (A1924T)	497 ± 32 *	-7.81 ± 0.09	2.1 ± 0.2	0.42 ± 0.02
apoCaM	3	1773-1940 (A1924T)	61 ± 4 *	-11.16 ± 0.14	-5.1 ± 0.3	0.70 ± 0.01

* $P < 0.05$ compared to $Na_V1.5$ CTD (amino acids 1773-1940) plus Ca^{2+}/CaM

Nat Commun. Author manuscript; available in PMC 2015 March 18.

Author Manuscript Author Manuscript Author Manuscript Author Manuscript

Table 3

Thermodynamic parameters for CaM interaction with the $Na_V1.2$ CTD

Titrant	*N*	Cell	K_d (nM)	ΔH (kcal/mol)	ΔS (cal·mol^{-1}·deg^{-1})	N value
apoCaM	3	WT	36 ± 6	-4.54 ± 0.1	18.6 ± 0.2	1.02 ± 0.02
Ca^{2+}/CaM	3	WT	1713 ± 333	6.01 ± 0.5	47.0 ± 1.3	0.76 ± 0.02
Ca^{2+}/CaM_{34}	3	WT	388 ± 22	-13.85 ± 0.4	-17.9 ± 1.4	0.86 ± 0.05
apoCaM	3	R1902C	958 ± 80 *	-3.28 ± 0.3	-2.1 ± 0.2	0.58 ± 0.13
Ca^{2+}/CaM	3	R1902C	1510 ± 187	6.19 ± 0.9	48.0 ± 2.8	0.74 ± 0.03
Ca^{2+}/CaM_{34}	3	R1902C	2931 ± 123 *	-12.53 ± 0.9	17.4 ± 2.8	0.49 ± 0.02

* $P < 0.05$ compared to WT.